J Mater Sci (2009) 44:6020–6027
DOI 10.1007/s10853-009-3811-2

Mechanical behavior of anodic alumina coatings reinforced with carbon nanofibers

Abhishek K. Kothari · Erkan Konca · Brian W. Sheldon · Kengqing Jian · Hao Li · Zhenhai Xia · Wangyang Ni · Robert Hurt

Received: 12 December 2008 / Accepted: 14 August 2009 / Published online: 2 September 2009

Abstract Anodic alumina was reinforced with three types of carbon nanofibers differing in the orientation of their graphene structure—perpendicular to the fiber axis, and parallel to the fiber axis both with dense core and hollow core (i.e., nanotubes). This study was designed to identify potential toughening and damage tolerant mechanisms in these nanoscale fiber-reinforced composite coatings. The dense carbon fibers improved contact damage resistance and reduced frictional resistance in sliding contacts. The hollow core reinforcements were much more promising for improving the fracture toughness of the composite coatings.

A. K. Kothari · B. W. Sheldon (✉) · K. Jian · R. Hurt
Division of Engineering, Brown University, Providence, RI 02912, USA
e-mail: Brian_Sheldon@brown.edu

A. K. Kothari
e-mail: Kothari81@gmail.com

E. Konca
Materials Engineering Department, Atilim University, Incek, Ankara 06836, Turkey

H. Li
Mechanical and Aerospace Engineering, University of Missouri at Columbia, Columbia, MO 65211, USA

Z. Xia
College of Engineering, The University of Akron, Akron, OH, USA

W. Ni
Materials and Processes Lab, Research and Development, General Motors, Warren, MI, USA

Introduction

Nanofibers have significant potential for enhancing the mechanical properties of ceramic coatings, where standard fiber reinforcements (diameters of tens to hundreds of microns) are too large to be useful. Nanofibers can serve as high-aspect ratio reinforcements because their diameters are much smaller than typical coating thicknesses. The fabrication processes used for many coatings are also more amenable for producing composites with relatively high nanofiber volume fractions, compared with bulk ceramic fabrication methods which are often limited to relatively low volume fractions. With this in mind, three different types of nanofibrous carbon reinforcements were used to explore possible approaches for improving the mechanical properties of anodized aluminum oxide (AAO) coatings.

Electrochemical anodization to produce AAO is a common method for modifying the surface properties of Al and related alloys [1–3]. It is also well established that nanostructured pores can be formed in AAO through proper control of the anodization process [4–7]. In recent years, these structures have been widely used as templates for growing carbon nanotubes (CNTs) and other nanofibrous materials [6, 8, 9]. The templates are often removed to create CNT arrays that can be used for other purposes [10]. However, the synthesis process also suggests the possibility of using the nano-reinforcements to improve the properties of the AAO. Because, the pores in CNT-reinforced AAO are generally normal to the substrate, these coatings are uniaxially reinforced. As noted previously, this configuration simplifies the interpretation of some of the mechanical properties measurements [11] which are difficult to test in nanocomposites [12].

The primary motivation for the research reported here was to compare the mechanical properties of AAO

reinforced with dense carbon nanofibers (CNFs) to similar materials produced with CNTs. Recent study demonstrates that nanofibrous reinforcements can be used to improve the elastic modulus and hardness of amorphous silica [13–15]. Previous study with AAO also demonstrates that CNTs can improve toughness [16, 17], which is particularly important, since the inherently low toughness of ceramics is often a limiting factor. Other mechanical properties besides toughness were also investigated here, primarily to provide initial information about using nanofiber-reinforced AAO as wear resistant coatings for Al alloys. The potentially low cost of the synthesis method used for the CNF reinforcements was also an important motivation for this study.

Description of experiments

Composite fabrication

Composite coatings were fabricated in two steps. First, porous AAO templates were produced by anodizing an aluminum substrate. This was followed by the templated growth of carbon nanostructures into the AAO, to essentially produce composite coatings on the Al alloy substrates.

For this study, mechanically polished 5657 Al alloy (~1% Mg, ~0.1% Cu, ~0.8% Si) specimens were anodized in 160 g/L of sulfuric acid solution at 18 °C, using a current density of 27.0 mA/cm^2 [4, 5]. This coating was then treated in 5 wt% H3PO3 solution at 34 °C for 4 min to obtain pores of 20–50 nm diameter. These AAO materials contain through thickness pores, as seen in Fig. 1. For the materials investigated here, the thickness of the anodic alumina was ~10 or ~80 μm. The thicker specimens were primarily used for nanoindentation studies on the side of the coatings, which are described further in the "Mechanical behavior" section. In several cases, composites were also fabricated with commercially available AAO filters with ~200 nm diameter pores (Anodisc, Whatman International Ltd., Kent, UK).

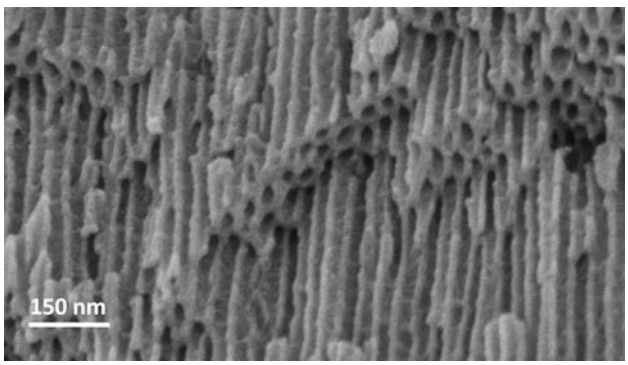

Fig. 1 Cross-sectional SEM image of anodized alumina showing through thickness pores

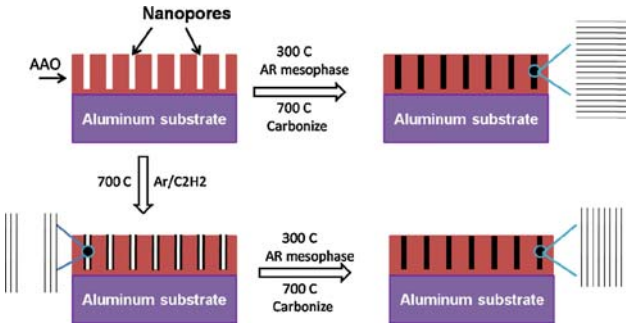

Fig. 2 Schematic description of fabrication steps to reinforce AAO with three different graphitic structures

The AAO coatings were used to produce carbon-reinforced composites. This was accomplished by growing three different types of carbon nanostructures in the pore structure of the alumina, as outlined below and summarized in Fig. 2.

Multiwall carbon nanotube-reinforced AAO coatings

The templates were first immersed in 0.1 M nickel nitrate (Ni(NO3)2) solution, to provide catalyst for CNT growth. They were then exposed to Ar (160 sccm) and hydrogen (80 sccm) gas at 600 °C for 30 min, which was followed by the addition of acetylene (60 sccm) for another 20 min. This produced multiwall carbon nanotubes (MWCNTs) in the pores via the catalytic decomposition of acetylene, a process that has been documented by other researchers [6, 9]. These samples will be referred to as CNT AAO in the rest of this study.

CNFs (with orthogonal graphene structures) reinforced coatings

These coatings were prepared by liquid capillary infiltration of AR mesophase pitch (HP grade, Mitsubishi Gas Chemical, New York, USA), which is a liquid crystalline homopolymer of naphthalene through the pores at 300 °C, followed by carbonization at 700 °C. In general, molecular interactions between the carbon precursor and the alumina walls determine the orientation of the graphene layers in the resulting material (i.e., roughly parallel or perpendicular to the fiber axis) [18]. In AAO templates, "edge-on" anchoring has been observed where the pitch interaction with the pore walls results in graphene planes that are oriented perpendicular to the fiber axis [8]. To verify this structure, lattice fringe images of the fibers were obtained with transmission electron microscopy. Here, the AAO was etched away with NaOH and the resulting solution was then dispersed on a Cu grid that was subsequently loaded into the microscope. Material reinforced with the type of nanofibers shown in Fig. 3a will be referred to as ortho-CNF AAO.

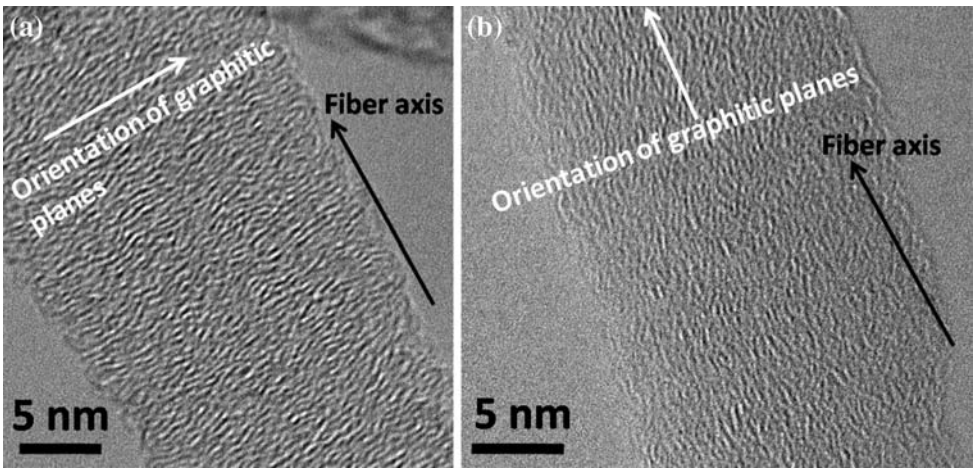

Fig. 3 Lattice fringe image showing graphitic planes **a** transverse to the fiber axis for ortho-CNF; **b** parallel to the fiber axis for hyb-CNF

Hybrid CNFs-reinforced coatings

The graphene layers in the pitch-derived nanofibers can also be engineered to be parallel to the fiber axis [19]. This was accomplished by first depositing a thin layer of pyrolytic carbon on the pore walls (similar to the MWCNT fabrication process described above), and then employing the liquid capillary infiltration method that was used to produce the ortho-CNF materials [8]. A lattice fringe image of this type of material is shown in Fig. 3b, where it is seen that the graphene planes are now aligned parallel to the fiber axis. Composites produced with these nanofibers will be referred to as hyb-CNF AAO. Figure 3a, b is a representative of more than 20 fibers imaged for each type of material, using 3 different coatings for each case.

Both the materials in Fig. 3b and the MWCNTs consist of graphene layers that are parallel to the fiber axis. The principal difference is the hollow core in the former, compared to the solid core in the latter. Schematic comparisons of the graphene planes in all three of the reinforcement materials are shown schematically in Fig. 2.

Mechanical behavior

All of the tests outlined below used unreinforced AAO as a reference material. Because, the composite fabrication methods exposed the AAO to the temperatures of 600–700 °C, all of the unreinforced AAO specimens used for mechanical testing were heat treated at 700 °C in Ar (160 sccm) and H_2 (80 sccm) flow for a baseline comparison. While the as-synthesized anodic alumina is amorphous, these heat treatments induce some crystallization (X-ray diffraction showed γ and δ-alumina, which is consistent with previous results for heat treated AAO [20, 21]).

The carbon fabrication methods also produce excess carbon on the top surfaces. To remove this residual carbon, the coatings were first polished using 0.05 μm alumina particles suspended in water. The composites were then evaluated with indentation methods, and by measuring their frictional resistance to sliding contact.

To measure the hardness and elastic modulus of the reinforced AAO and annealed AAO, load versus displacement curves were obtained by nanoindentation (using a Berkovich tip, with a Nanoindenter XP). The unloading curves were then analyzed with the procedure developed by Oliver and Pharr [22].

To look for evidence of toughening mechanisms, indentation was conducted using a cube-corner tip and higher loads. These investigations were conducted by indenting the side of thicker coatings. The coatings were mounted sideways in epoxy and polished using fine alumina solution. The resulting indentations and cracking were then examined with scanning electron microscopy (SEM).

The friction response was investigated in sliding contact with 6.35 mm diameter WC–Co balls, in a ball-on-disc tribometer. These tests were performed under 1 N load in ambient air (40% relative humidity).

Results

Elastic modulus and indentation hardness

The nanoindentation data were collected at several locations on each coating and the average values and the standard deviation are reported in Table 1. These data show that the reinforced AAO coatings are harder and stiffer than the matrix material (unreinforced, annealed AAO). However, there is not a significant variation in mechanical properties among the AAO coatings reinforced with different carbon nanostructures. In particular, the different graphene orientational patterns in the two dense nanofiber types might be expected to influence mechanical properties through the intrinsic anisotropy of the graphene

Table 1 Summarized nanoindentation results of reinforced-AAO as compared to AAO

Sample	Hardness (GPa)	Modulus (GPa)
AAO	2.1 ± 0.1	57 ± 3
AAO-annealed	3.3 ± 0.2	59 ± 3
Ortho CNF-reinforced AAO	5.6 ± 0.3	82 ± 3
hybCNF-reinforced AAO	5.1 ± 0.3	74 ± 4
MWCNT-reinforced AAO	5.5 ± 0.5	80 ± 4

building block. The similarity in their properties may be associated with graphene layer disorder, especially the small layer dimension associated with low carbonization temperature. Typically, mechanical anisotropy in liquid-crystal-derived carbons increases greatly with high-temperature annealing, which increases the mean layer size and narrows the orientational distribution. The primary effect is the development of higher strength and stiffness along the axis parallel to the layer planes. In the case of MWCNTs, the more ordered graphene layers should lead to higher axial stiffness; however, the hollow core should reduce the overall stiffness, normalized to the total radius of the reinforcement (i.e., to at least some extent, these two effects should offset each other). This trade-off provides a possible explanation for the similar hardness and modulus values that were observed with the coatings reinforced with MWCNTs and dense nanofibers.

Crack deflection and interface debonding

Cube corner indentation of the top surfaces of these materials provides basic information about deformation behavior. Xia et al. [16] previously conducted a similar study with different diameter MWCNTs (in different sized AAO pores), where the indentation response showed significant differences associated with the tube diameter and wall thickness. In particular, indentation produced cracking in AAO reinforced with ~50 nm diameter MWCNTs, whereas cracking was not observed when identical indentation was done on the unreinforced matrix and in AAO reinforced with MWCNTs that had somewhat larger diameters and thinner walls [16].

The AAO matrices used for most of this study have a somewhat different composition and smaller pores than the materials used by Xia et al. [16]. To provide a wider variation in the reinforcement diameter, we also made limited comparisons with composites produced from the commercially available AAO templates (~200 nm diameter pores). Figure 4a shows an indentation crack that was generated on the top surface of this type of large pore hybCNF AAO composite using a 0.4-N load, and the arrows in Fig. 4b point to clear evidence of crack deflection and interface debonding. These behaviors were not observed in any of the AAO coatings with smaller diameter (20 nm) carbon reinforcements, even with much larger loads of 3 N. For example in Fig. 4c, there is no radial crack emanating from the indent. The indentation parameter $(P_V * H^3/K_{Ic}^4)$ for these composites was estimated to be greater than 3.8×10^5, where P_V, H, and K_{Ic} are the applied load (3 N), hardness (~5 GPa), and mode I fracture toughness (<1 MPa $m^{1/2}$) [17], respectively. Although there is uncertainty in the value for K_{Ic}, this estimated indentation parameter is an order of magnitude higher than the 'universal threshold parameter' of 1.5×10^4 [23]. This implies that these indentation conditions were not sub-threshold, i.e., the indentation loads are large enough to generate cracks. This is consistent with similar testing on the unreinforced AAO matrix, where indentation cracks were observed at loads of only 0.4 N, as seen in Fig. 4d.

As noted above, resistance to contact damage was also observed in prior work with MWCNT-reinforced AAO with somewhat larger pores [16]. However, in this earlier study similar indentation loads did not lead to cracking in the unreinforced material, and contact damage resistance was attributed at least in part to collapse of the nanopores in the unreinforced material, and to the collapse of the pores and MWCNTs in the reinforced material. Thus, the current materials are significantly different, since the unreinforced material cracks more easily here and also because the dense carbon fibers do not collapse or buckle as the MWCNTs did. In making this comparison, note that the composition of the anodic alumina fabricated here differs from the anodic alumina used in the previous study by Xia et al. [16]. In particular, this prior study used high-purity Al for anodization, instead of the 5657 Al alloy. Thus, differences in the mechanical properties of the AAO are likely to be related to differences in the oxide composition, in addition to the effects of the smaller pore sizes in the current material.

Qualitative toughness evaluation

Enhanced toughening in ceramic matrix composites is generally associated with interface debonding, crack bridging by fibers, and fiber pull-out. Evidence for these mechanisms is often obtained by examining fracture surfaces. With this in mind, indentation cracks were introduced on the side of the ~80-μm thick composite AAO coatings. As seen in Fig. 5, these indentation cracks were roughly transverse to the axial direction of the fibers, using loads of 50–200 mN. These loads are significantly lower than those used to generate the cracks described in "Crack deflection and interface debonding" section, which again reinforces the conclusion that a different type of damage resistant behavior is apparently activated on the top surfaces.

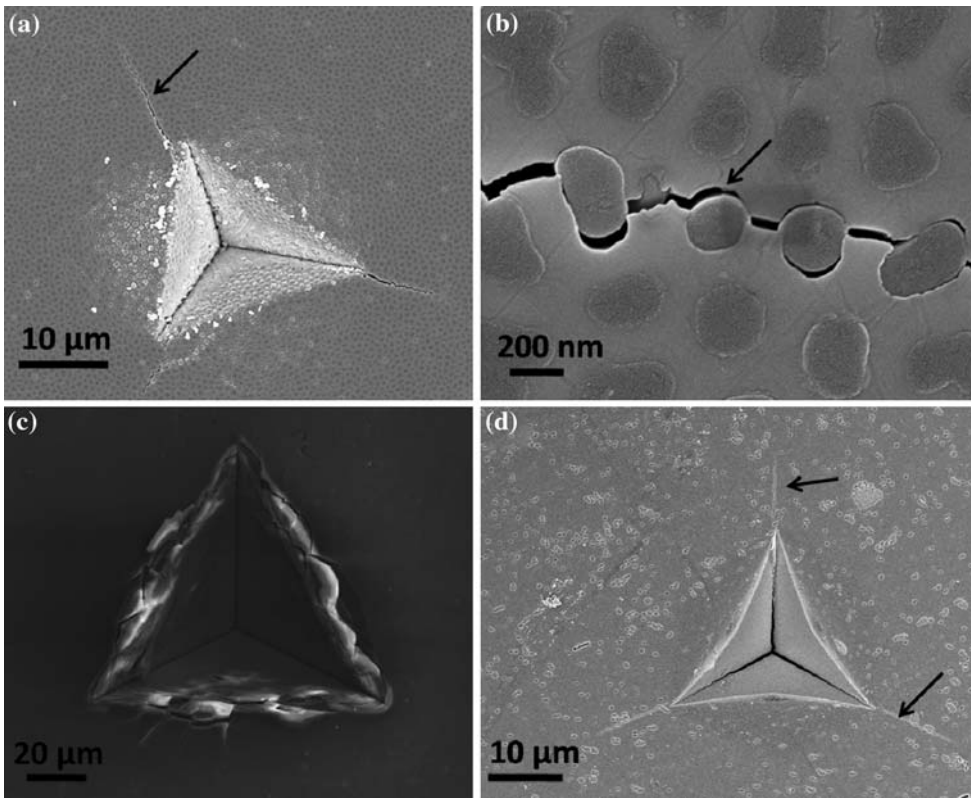

Fig. 4 SEM images showing **a** presence of cracks when the CNF (of 200 nm diameter) reinforced coating was indented with 0.4 N load; **b** higher-magnification image of the region marked with *arrow* in (**a**) showing crack deflection around carbon fibers. *Arrows* indicate the sites of debonding; **c** absence of cracks emanating from the residual indent impression on smaller diameter CNF (of 20 nm diameter) reinforced AAO coatings even at 3 N load. There is no delamination at the center of the impression instead smaller cracks are observed along the periphery of the impression; **d** cracks emanating from the residual indent impression on AAO coating (*arrows*). There is also sign of coating delamination evident at the center of the impression

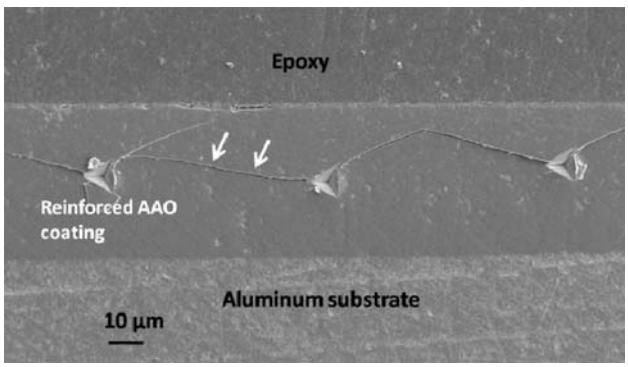

Fig. 5 SEM image showing a range of indentations made on the sideways mounted coating to observe the toughening mechanism in reinforced AAO coatings (identical arrangement for all reinforced coatings). *Arrows* indicate cracks coming out of the residual indent impression

The MWCNT AAO shows clear evidence of crack bridging, as seen in Fig. 6a. This is consistent with prior study on nanotube-reinforced AAO [11, 16], and it indicates that the nanotubes increase the coating toughness. However, fracture surfaces of both the ortho-CNF AAO (Fig. 6b) and the hyb-CNF AAO (Fig. 6c) indicate that these reinforcements fracture along roughly the same plane as the matrix, without any substantial pull-out. This implies that the CNF materials do not provide comparable toughening.

Friction response

The frictional behavior for all of the materials is shown in Fig. 7. In all cases, the coefficient of friction (COF) decreased to an apparently steady-state value relatively quickly. All three of the composites exhibit COF values that were nearly one-third of the values for the annealed AAO and untreated Al surfaces. This substantial decrease suggests that the nanocarbon reinforcements significantly reduce friction. Since graphitic carbon is a common solid lubricant, this result is not entirely surprising. The COF for CNT AAO is higher than the CNF composites, which is perhaps associated with the lower carbon volume due to the CNT hollow core. Otherwise, the limited nature of these experiments does not provide enough information to further assess differences in the way that these nanocarbons influence friction. However, based on the relatively low COF values observed with the composites, a more detailed study of friction is warranted.

Discussion and conclusions

The two types of CNF-reinforced AAO showed fairly similar mechanical properties in all of the tests reported here. In the ortho-CNFs, the graphene layers are roughly perpendicular to the fiber axis, and hence parallel to the

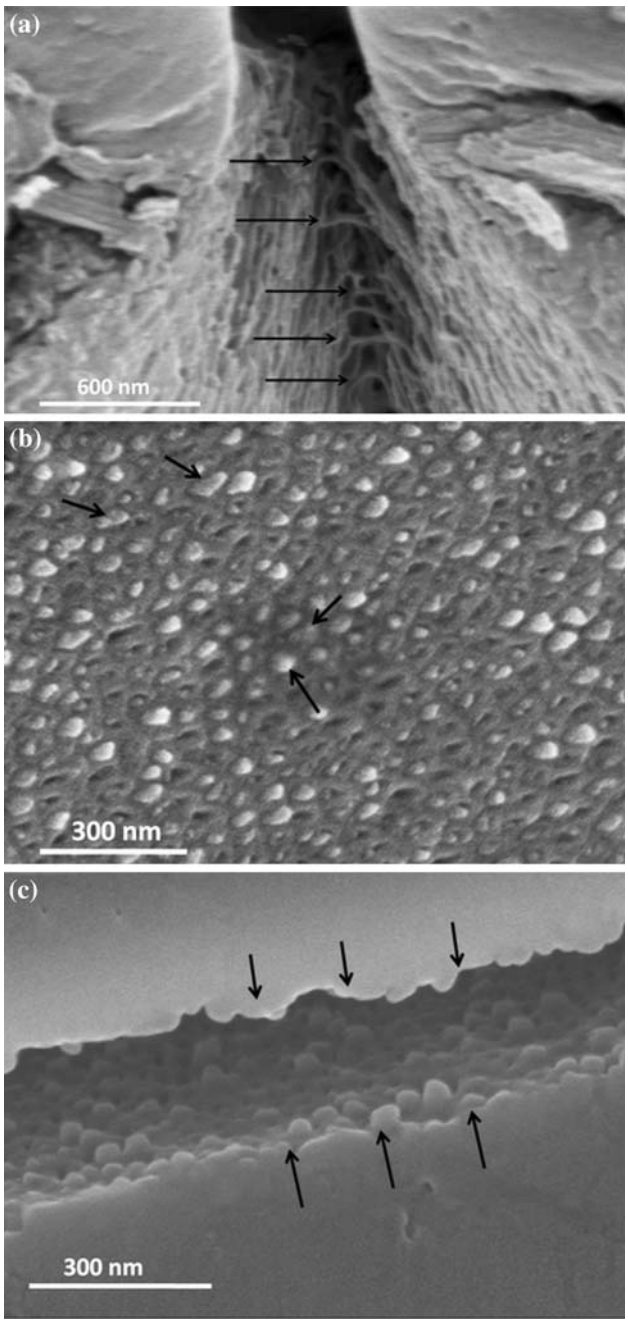

Fig. 6 Fracture surface of **a** MWCNT-reinforced AAO showing crack bridging by the nanotubes. *Arrows* indicate the location of fibers fractured along with the matrix; **b** ortho-CNF-reinforced AAO showing no pull-out; **c** hyb-CNF-reinforced AAO again showing absence of bridging by the fibers and there is absence of pull-out in the crack wake

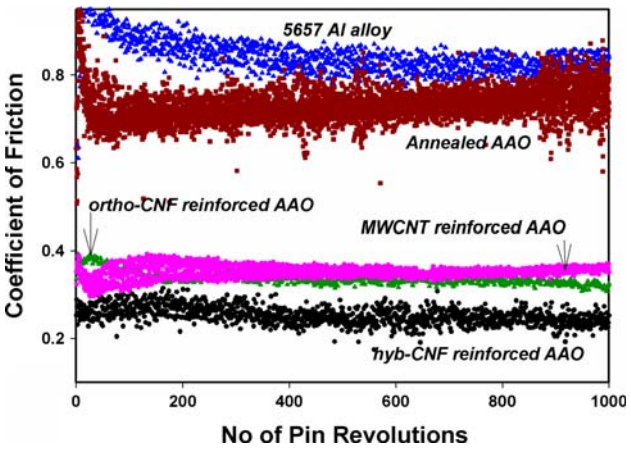

Fig. 7 Friction response of reinforced AAO in comparison with annealed AAO and Al alloys itself clearly showing that carbon nanostructures can substantially lower the frictional resistance of the coating

cracks. Because, the carbon bonding is relatively weak between the graphitic planes, these structures are not well configured to resist crack propagation. Hence, the absence of pull-out with the ortho-CNFs was expected. However, the lack of pull-out observed in the hyb-CNF AAO materials was probably the most unexpected observation in this study, especially since significant pull-out occurred when using CNTs with similar graphene ordering. The only significant difference between these two reinforcements is the hollow core in the CNTs versus the solid core in the hyb-CNFs. This difference in structure seems to favor nanotubes as a toughening agent. Nanotubes have a flexible structure due to their hollow core and are thus capable of deforming much more easily in the radial direction, compared to similarly structured nanofibers with a solid core. This difference could lead to significantly more pull-out with MWCNTs, by allowing the nanotubes to accommodate non-uniformities that would otherwise generate very high interfacial sliding resistance. For example, interfacial roughness between the reinforcement and the AAO matrix will generally increase friction during pull-out; however, this effect should be less pronounced with hollow nanotubes that deform more readily as they slide past interfacial asperities. It is also possible that the hollow core of the nanotubes leads to higher variability in tensile strength. This cannot be easily verified experimentally; however, the complete absence of pull-out from the fracture surfaces in the hyb-CNF material casts doubt on this argument.

The toughening benefit of the MWCNT hollow core has also been recently observed in similar pull-out observations with amorphous silicon nitride matrices [24]. In this case, the nitride fabrication process should produce stronger bonding between the matrix and the carbon reinforcements, and the MWCNTs still showed substantial pull-out. In contrast, hyb-CNFs that were heat treated to 2500 °C to obtain a well-ordered graphitic structure still showed almost no pull-out from the silicon nitride matrix.

The comparison between the different reinforcements sheds some light on toughening mechanisms in carbon nanostructures. This may be particularly relevant to the

design of other nanoscale fiber-reinforced composite systems. In general, the arrangement of graphene layers in the reinforcement should affect the properties of the resultant composite. However, low temperature-derived CNFs appear to have mechanical properties that are not strongly dependent on the graphene layer alignment with respect to the fiber axis. The minimal impact of these structural effects can be contrasted with the observed differences in toughening and deformation that appears to be induced by the hollow core of the MWCNTs. In ceramic composites, it is also well established that the interface properties (between the matrix and reinforcements) are critical. In previous study with MWCNT-reinforced AAO, some evidence suggests that the primary interaction between AAO and the CNTs is through frictional coupling (i.e., chemical bonding at the interface is very limited or perhaps nonexistent). Residual stress analysis on these materials by Xia et al. [16] showed the thermal expansion mismatch between MWCNT and AAO resulted in hoop tension, radial compression, and axial tension in the matrix material. Stronger chemical bonding between the matrix and nanocarbon reinforcements' fibers should also be possible, with proper functionalization of the surfaces during synthesis. Further investigation of these effects and possibilities is clearly warranted.

The improved contact damage resistance of the CNF composites was also not completely expected. Homogeneous and heterogeneous ceramics respond to contact loading in fundamentally different ways [23, 25]. In homogeneous ceramics, the intense confined shear under the sharp indenter tip produces anelastic deformation, and the elastic/anelastic mismatch results in the formation of radial cracks [23]. Highly heterogeneous ceramics also undergo anelastic deformation. However, if they are sufficiently weak in shear, considerable redistribution of stresses can take place under the indenter, resulting in the suppression of long cracks. CNFs-reinforced AAO coatings thus seem to exhibit contact damage tolerance which is related to the properties and dimensions of the constituent phases. This may present new opportunities for ceramic composites which are increasingly being used in applications where high contact loading exists, such as bearing, valves, nozzles, seals, armor, and also in biomedical applications.

Although the CNFs did not provide toughening, the other properties reported here demonstrate that nanocarbon reinforcements can substantially improve the properties of AAO coatings. In particular, the combination of increased hardness, improved resistance to contact damage, and decreased friction all imply that these composites will exhibit improved performance in applications where wear resistance is important. Thus, anodized Al alloys that are reinforced with CNFs appear to provide a cost effective method for improving the surface mechanical properties of commercially important Al alloys.

It is also important to keep in mind that the graphene layers in all of the materials studied here contain significant disorder, where the graphitic regions are limited in size. While they are oriented along a preferred axis, the individual layers show statistical angular distributions around this axis, which is typical of liquid-crystal-derived carbons formed at low carbonization temperatures [19]. Variations in the carbon structure of both CNFs and CNTs may yet lead to a broad range of properties, well beyond those reported here. In particular, the variations in the bonding between graphene layers should have a significant impact on toughening mechanisms. A wide range of properties are also known to exist for AAO materials that are fabricated under different conditions, and as noted above the interfaces between the matrix and the reinforcements can be engineered in different ways. Thus, there appear to be a very wide range of nanocarbon-reinforced AAO coatings that can be explored further.

Acknowledgement Financial support from NSF-NIRT Grant No. CMS-03034246 is highly appreciated.

References

1. Wu XH, Qin W, Cui B, Jiang ZH, Lu WQ, He WD (2008) J Mater Process Technol 200:405
2. Grillet AM, Gorby AD, Trujillo SM, Grant RP, Hodges VC, Parson TB, Grasser TW (2008) J Colloid Interface Sci 317:264
3. Wang H, Wang HW (2007) Appl Surf Sci 253:4386
4. Masuda H, Fukuda K (1995) Science 268:1466
5. Li AP, Muller F, Birner A, Nielsch K, Gosele U (1998) J Appl Phys 84:6023
6. Jeong SH, Hwang HY, Hwang SK, Lee KH (2004) Carbon 42:2073
7. Pancholi A, Stoleru VG, Kell CD (2007) Nanotechnology 18:8
8. Jian KQ, Shim HS, Schwartzman A, Crawford GP, Hurt RH (2003) Adv Mater 15:164
9. Che G, Lakshmi BB, Martin CR, Fisher ER, Ruoff RS (1998) Chem Mater 10:260
10. Li J, Papadopoulos C, Xu JM, Moskovits M (1999) Appl Phys Lett 75:367
11. Xia Z, Riester L, Sheldon BW, Curtin W, Liang J, Yin A, Xu JM (2004) Rev Adv Mater Sci 6:131
12. Sheldon BW, Curtin WA (2004) Nat Mater 3:505
13. Luo JT, Wen HC, Chou CP, Wu WF, Wan BZ (2007) J Compos Mater 41:979
14. Boccaccini AR, Thomas BJC, Brusatin G, Colombo P (2007) J Mater Sci 42:2030. doi:10.1007/s10853-006-0540-7
15. Callone E, Fletcher JM, Carturan G, Raj R (2008) J Mater Sci 43:4862. doi:10.1007/s10853-008-2707-x
16. Xia Z, Riester L, Curtin W, Li H, Sheldon BW, Liang J, Chang B, Xu JM (2004) Acta Mater 52:931
17. Xia Z, Curtin WA, Sheldon BW (2004) J Eng Mater Technol Trans ASME 126:238
18. Hurt R, Krammer G, Crawford G, Jian KQ, Rulison C (2002) Chem Mater 14:4558

19. Chan C, Crawford G, Gao Y, Hurt R, Jian K, Li H, Sheldon BW, Sousa M, Yang N (2005) Carbon 43:2431
20. Kirchner A, MacKenzie KJD, Brown IWM, Kemmitt T, Bowden ME (2007) J Membr Sci 287:264
21. Santos PS, Santos HS, Toledo SP (2000) Mater Res 3:104
22. Oliver WC, Pharr GM (1992) J Mater Res 7:1564
23. Lawn BR (1993) Fracture of brittle solids. Cambridge University Press, Cambridge
24. Kothari AK, Jian KQ, Rankin J, Sheldon BW (2008) J Am Ceram Soc 91:2743
25. Lawn BR, Padture NP, Cai H, Guiberteau F (1994) Science 263:1114